NRL Report 8258

Fractographic Analysis of Fatigue Specimens of Annealed Type 304 Stainless Steel

V. PROVENZANO AND F. A. SMIDT, JR.

Thermostructural Materials Branch
Material Science and Technology Division

September 21, 1978

NAVAL RESEARCH LABORATORY
Washington, D.C.

tested at 593°C (1100°F) showed a change in failure mode to partially intergranular failure and an increase in the crack growth rate relative to tests at 427°C. Imposition of a hold time up to 1 min further increased the proportion of the fracture surface characterized by intergranular failure, and the crack growth rate also increased. The material that had been aged at 593°C and tested at 427°C and at 593°C showed a return to transgranular failure. The crack growth rate in the aged material tested at 427°C was comparable to that of the SA material tested at the same temperature, while the growth rate of the aged material at 593°C was somewhat higher than at 427°C. Twenty-five percent cold-worked material tested at 593°C with 1-min hold time showed an intergranular failure mode for all values of ΔK and a crack growth rate higher than the one found in the SA material for the same set of test conditions. Twenty-five percent cold-worked material aged and tested at 593°C for hold times up to 1 min exhibited mixed failure mode, while the corresponding fatigue data showed a reduced hold-time effect compared to the one observed in the mechanical data of the 25% cold-worked specimens.

The above observations were consistent with a model in which the grain boundaries were embrittled by diffusion of oxygen ahead of the crack tip, resulting in intergranular failure and an increased crack growth rate. Thermal aging led to precipitate formation, which impeded grain boundary sliding and reduced the extent of intergranular failure. The cold-work treatment, by contrast, appeared to strengthen the matrix material relative to the grain boundaries so that intergranular failure was more likely to occur.

CONTENTS

FRACTOGRAPHIC ANALYSIS OF FATIGUE SPECIMENS OF ANNEALED TYPE 304 STAINLESS STEEL

INTRODUCTION

The present work is part of a continuing effort to develop an understanding of the fatigue behavior of nickel-base alloys and austenitic stainless steels in high-temperature structural applications. It deals with the fatigue behavior of Type 304 stainless steel and was conducted in parallel with a similar study on Type 316 stainless steel (1).

In the present study, the fracture surfaces of Type 304 stainless steel specimens that had previously been fatigue-tested in air were examined by scanning electron microscopy (SEM). The specimens were generously provided by Shahinian and Michel from previous studies (2-4) of the fatigue behavior of the austenitic stainless steels as a function of test temperature, material condition, and hold time in single-edge-notched cantilever beam specimens cycled under zero-to-tension loading in air. As with the previous SEM study on Type 316 stainless steel (1), the basic aim of this work was to gain additional insight into the mechanisms of elevated-temperature fatigue failure.

A fundamental problem of understanding fatigue behavior at high temperature is the separation of time-dependent deformations, such as creep, from the cyclic-dependent fatigue processes. Test temperature, test environment, the thermomechanical history of the material, applied stress, etc., all may influence, to a greater or a lesser degree, the fatigue behavior of the material being investigated. A number of these variables were examined in this study in an effort to increase our understanding of high-temperature fatigue behavior.

The sequence of presentation is to first briefly review the experimental procedures under which the fatigue data were obtained and the SEM techniques used to examine the specimens' surfaces; next, to present the SEM observations in the context of the fatigue history for each specimen; then, to present a discussion and interpretation of the results for each set of material history/test condition that exhibited a unique response; and finally, to summarize with conclusions and implications.

EXPERIMENTAL PROCEDURE

Single-edge-notched cantilever beam specimens were cycled under zero-to-tension loading to a constant maximum load in air at temperatures of 427 and 593°C (800 and 1100°F). The nominal loading frequency (without a hold-time period) was 0.17 Hz (10 cpm) with a sawtooth waveform. The effect of static loading (hold time) was examined by holding the maximum load for 0.1 and 1.0 min before returning to zero load.

Manuscript submitted June 28, 1978.

Two heats of Type 304, designated A and B, were used in this study, and their compositions are given in Table 1. Material conditions examined included material solution-annealed (SA) at 1090°C (2000°F) for 1 h and material aged 5000 h in air at 593°C.

Table 1 — Chemical Composition of Type 304 Stainless Steel in Weight Percent

Element	C	Mn	P	S	Si	Cr	Ni	Mo	Cu
Heat A	0.048	1.48	0.025	0.015	0.52	18.57	9.45	—	—
Heat B	0.048	1.18	0.032	0.016	0.48	18.56	9.80	0.31	0.22

The SEM specimens examined were machined to approximately 20.0 mm X 9.0 mm X 2.5 mm from failed fatigue specimens. A Coates and Welter 106A field emission scanning electron microscope was used for the fractographic examination of the specimens. Because the mechanical tests were conducted in air at elevated temperatures, the fracture surfaces were oxidized to varying degrees. It was therefore necessary to remove this oxide layer to observe the true fracture surface. An oxide removal technique using an inhibited HCl solution (5) (100 ml 6N HCl with 0.2g hexamethylene-tetramine) was developed and described in the previous study on Type 316 stainless steel (1), and the reader is referred to that study for additional details.

EXPERIMENTAL RESULTS

Several distinguishable types of failure behavior were identified from the SEM examination of AISI Type 304 stainless steel fatigue specimens. The failure modes appeared to be most strongly influenced by test temperature and thermomechanical history, but under certain conditions were also influenced by hold time. The results are presented in the following sequence of test conditions/material history combinations:

(a) Heat B, solution-annealed, tested at 427°C (for all hold times),
(b) Heat B, solution-annealed, tested at 593°C, (for all hold times),
(c) Heat B, solution-annealed, aged for 5000 h at 593°C, tested at 427°C (for all hold times),
(d) Heat B, solution-annealed, aged for 5000 h at 593°C, tested at 593°C (for all hold times),
(e) Heat A, solution-annealed, and solution-annealed and aged for 5000 h at 593°C, both material conditions tested at 593°C (for all hold times),
(f) Heat A, 25% cold-worked, and 25% cold-worked and aged for 5000 h at 593°C, both material conditions tested at 593°C.

The fatigue crack propagation data were analyzed and presented in the form of log da/dN (crack growth rate) vs log ΔK (stress intensity) curves in the original reports (2-4). These plots are included in the present report for easy reference and comparison. The curves were derived from graphic and computer analysis of the change in the crack length during a fatigue test,

and the ΔK values calculated for that crack length from the Gross and Srawley expression for stress intensity in pure bending (6). The results generally approximated a linear behavior when plotted as log da/dN vs log ΔK, and fell within a scatterband.

Heat B, Solution-annealed, Tested at 427°C

The crack growth rate plots (Fig. 1) show that most of the data for all hold times fall on a line which increases from a growth change rate per cycle of approximately 2×10^{-4} mm/cycle (5×10^{-6} in./cycle) at a ΔK of 22 MPa$\sqrt{m}$ (20 ksi$\sqrt{in.}$) to 1×10^{-2} mm/cycle (4×10^{-3} in./cycle) at about 88 MPa$\sqrt{m}$ (80 ksi$\sqrt{in.}$). This line has a slope of about 3. A minor change in slope occurs at a ΔK of about 55 MPa$\sqrt{m}$ (50 ksi$\sqrt{in.}$), but, as shown in the previous study on Type 316 stainless steel (1), changes in the slope in the high-ΔK region do not appear to be significant. A more significant exception to the straight-line trend band is the decrease in slope at 40 MPa$\sqrt{m}$ (36.4 ksi $\sqrt{in.}$) observed in the 1-min hold-time test.

Typical SEM micrographs of the SA material, Heat B, tested at 427°C without hold time are shown in Fig. 2. The fracture surface shows a transgranular mode of failure for all values of ΔK. Fatigue striations are clearly visible in all four micrographs. These striation markings are typical of those found in ductile metals (7) as a consequence of the alternate extension of the crack by shear and the subsequent compression of the crack tip region during the unloading part of the cycle.

Measurements of the striation spacing at both high and low ΔK show a close correlation with the calculated da/dN values. The striation spacing increases as higher growth rates per cycle and higher ΔK values are noted. This is illustrated by two high-magnification micrographs (Fig. 2, c and d). Imposition of a hold time up to 1 min produced no noticeable change in the appearance of the fracture surface, as can be seen in Fig. 3.

Heat B, Solution-annealed, Tested at 593°C

Crack growth rate data for 0, 0.1-, and 1-min hold times (2) are presented in Fig. 4. The crack growth rate for the specimen tested with no hold time increased from approximately 4.5×10^{-3} mm/cycle (2.3×10^{-4} in./cycle) at 22 MPa$\sqrt{m}$ (20 ksi$\sqrt{in.}$) to 3.5×10^{-3} mm/cycle (1.3×10^{-3} in./cycle) at 88 MPa$\sqrt{m}$ (80 ksi$\sqrt{in.}$). This crack growth rate is more than one order of magnitude higher than the growth rate of the same material tested at 427°C for comparable values of ΔK. The crack growth rate curves exhibits a small change in slope at 33 MPa$\sqrt{m}$ (30 ksi$\sqrt{in.}$) and another larger change in slope at 44 MPa$\sqrt{m}$ (40 ksi$\sqrt{in.}$). Introduction of 0.1- and 1.0-min hold times during the fatigue cycle increased the crack growth rate as compared to the test with no hold time. Similar to the zero-hold-time test, the two crack growth rate curves exhibit two changes in the slope at approximately the same values of ΔK. Since these changes in the slope occur in the region of ΔK where the mechanical data are most reliable, they cannot be easily discounted. This point will be taken up again in the discussion section of this report.

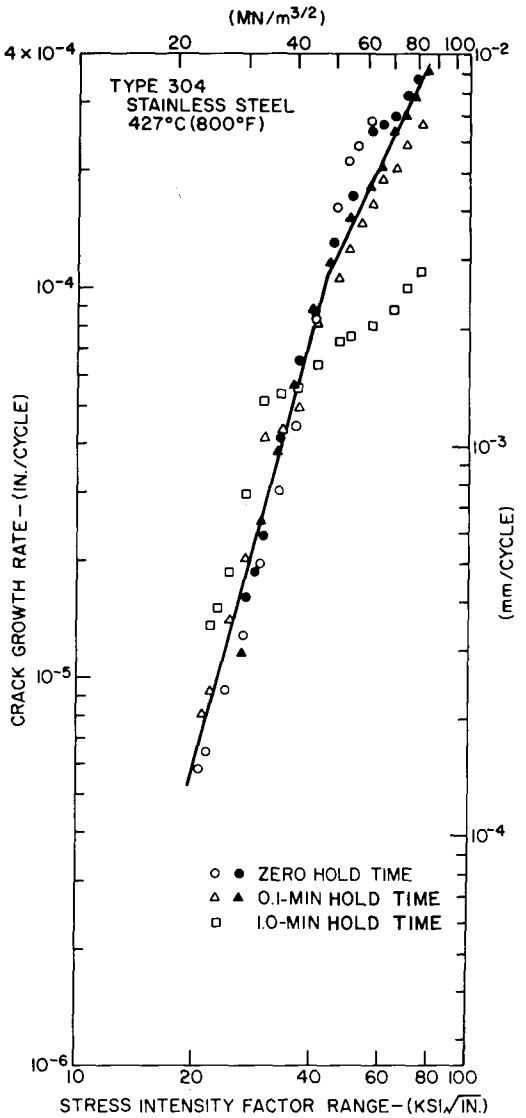

Fig. 1 — Effect of hold time on fatigue crack propagation rate, da/dN, in air at 427°C for solution-annealed Type 304 stainless steel, Heat B.

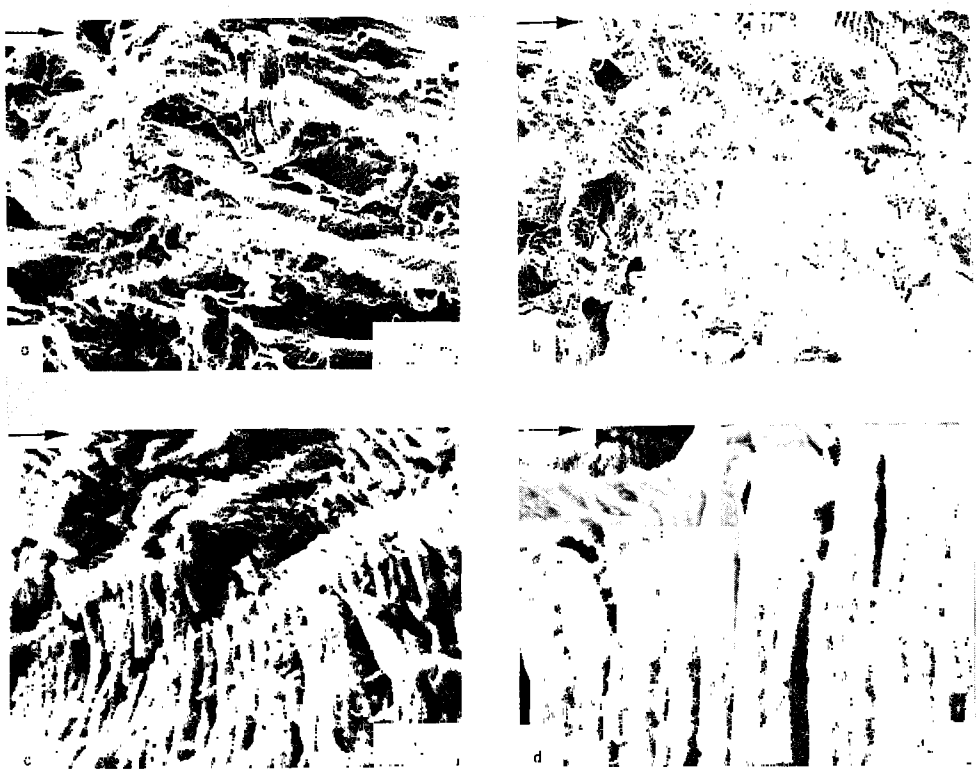

Fig. 2 — Fracture surfaces of a solution-annealed stainless steel specimen, Heat B, tested at 427°C with zero hold time. Arrows show direction of macroscopic crack propagation. The SEM micrographs were taken at crack lengths that correspond to the following ΔK values: (a) 22 MPa$\sqrt{m}$ (20 ksi$\sqrt{in.}$), (b) 44 MPa$\sqrt{m}$ (40 ksi$\sqrt{in.}$), (c) 22 MPa$\sqrt{m}$ (20 ksi$\sqrt{in.}$), and (d) 27.5 MPa$\sqrt{m}$ (25 ksi$\sqrt{in.}$). Transgranular features with fatigue striations are clearly visible in all four micrographs.

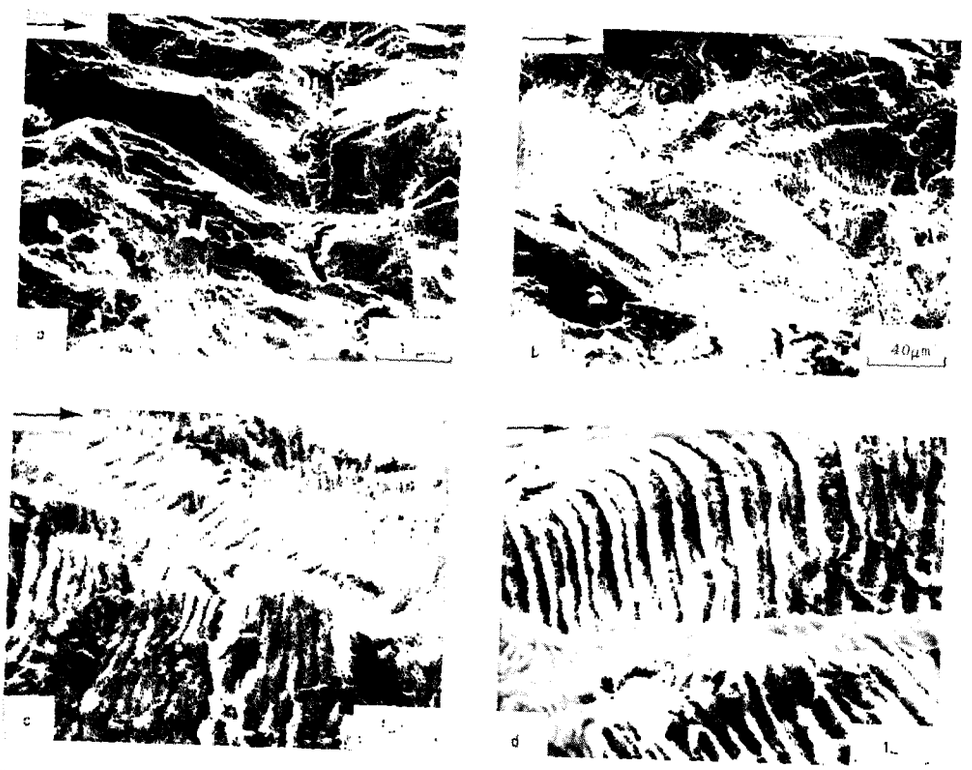

Fig. 3 — Fracture surfaces of a solution-annealed stainless steel specimen, Heat B, tested at 427°C with 1-min hold time. Arrows show direction of macroscopic crack propagation. The SEM micrographs were taken at crack lengths that correspond to the following ΔK values: (a) 22 MPa$\sqrt{m}$ (20 ksi$\sqrt{in.}$), (b) 44 MPa$\sqrt{m}$ (40 ksi$\sqrt{in.}$), (c) 22 MPa$\sqrt{m}$ (20 ksi$\sqrt{in.}$), and (d) 33 MPa$\sqrt{m}$ (30 ksi$\sqrt{in.}$). Similar to the micrographs shown in Fig. 2, the failure mode is transgranular with distinct fatigue striations whose average spacing increases with ΔK.

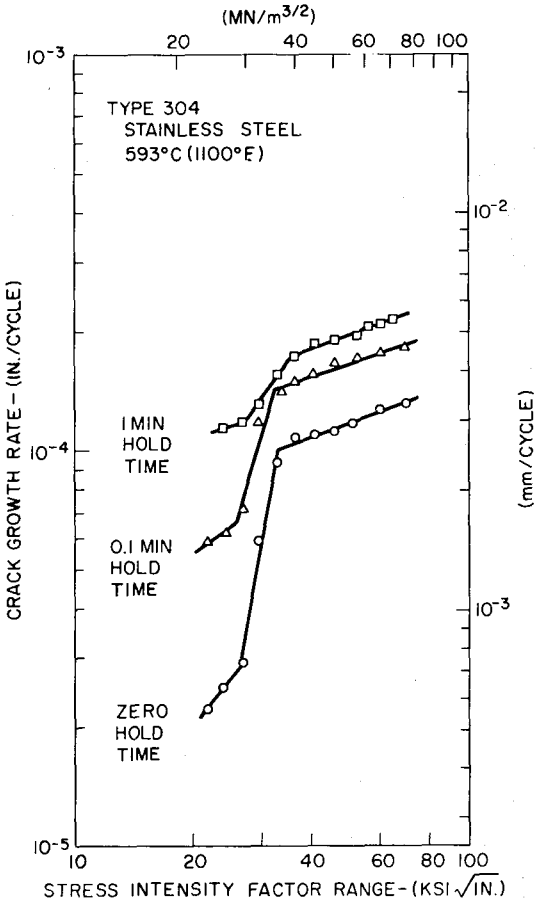

Fig. 4 — Effect of hold time on fatigue crack propagation rate, da/dN, in air at 593° for solution-annealed Type 304 stainless steel, Heat B.

Typical SEM micrographs of the SA specimen tested at 593°C with no hold time are shown in Fig. 5. As in prior figures, these micrographs include representatives from both low- and high-ΔK regions of the test. At crack lengths up to 10 mm (0.4 in.) (which corresponds to a ΔK value of 33 MPa$\sqrt{m.}$(30 ksi$\sqrt{in.}$)), the failure mode was mixed, as can be seen in Fig. 5, a and b. Some areas exhibit intergranular failure while others quite obviously show the characteristics of the transgranular failure mode. At ΔK levels above 33 MPa$\sqrt{}$(30 ksi$\sqrt{in.}$), the failure mode changed to 100% transgranular and fatigue striations are clearly visible (Fig. 5, c and d). The striation spacing correlates well with da/dN values calculated from the crack extension data. Behavior of this type was also noted in the previous study on Type 316 (1). The introduction of a 1-min hold time during the fatigue cycle increased the percentage of area characterized by intergranular failure and increased the ΔK level at which transgranular failure occurred, as can be seen in Fig. 6.

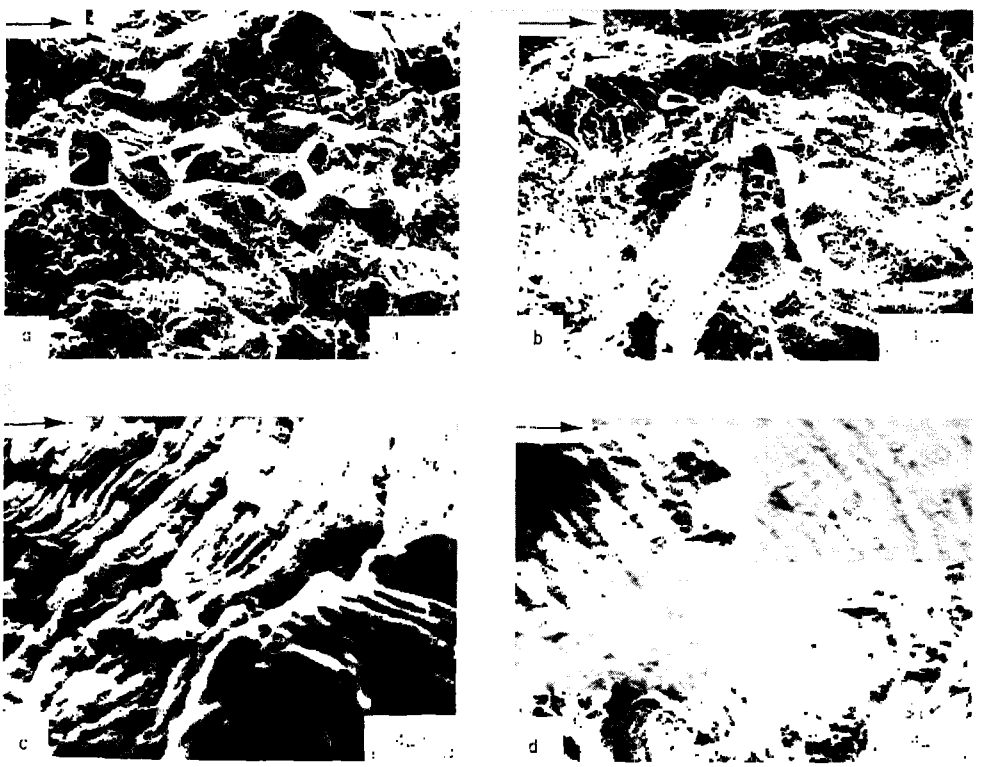

Fig. 5 — Fracture surfaces of a solution-annealed specimen, Heat B, tested at 593°C without hold time. The SEM micrographs were taken at crack lengths that correspond to the following ΔK values: (a) 22 MPa$\sqrt{m}$ (20 ksi$\sqrt{in.}$), (b) 27.5 MPa$\sqrt{m}$ (25 ksi$\sqrt{in.}$), (c) 33 MPa$\sqrt{m}$ (30 ksi$\sqrt{in.}$), and (d) 44 MPa$\sqrt{m}$ (40 ksi$\sqrt{in.}$). Arrows show direction of macroscopic crack propagation. The fracture mode is mixed — intergranular and transgranular — in the low-ΔK region and totally transgranular in the high-ΔK region.

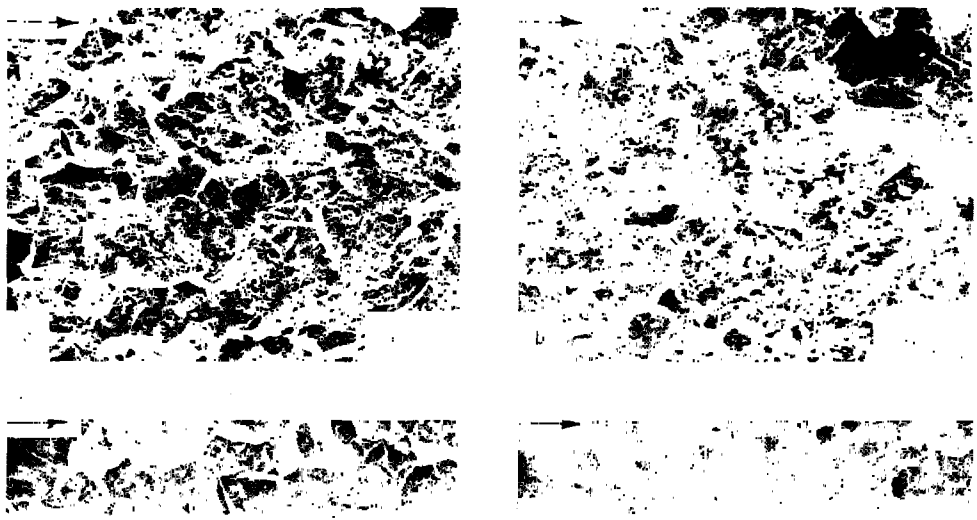

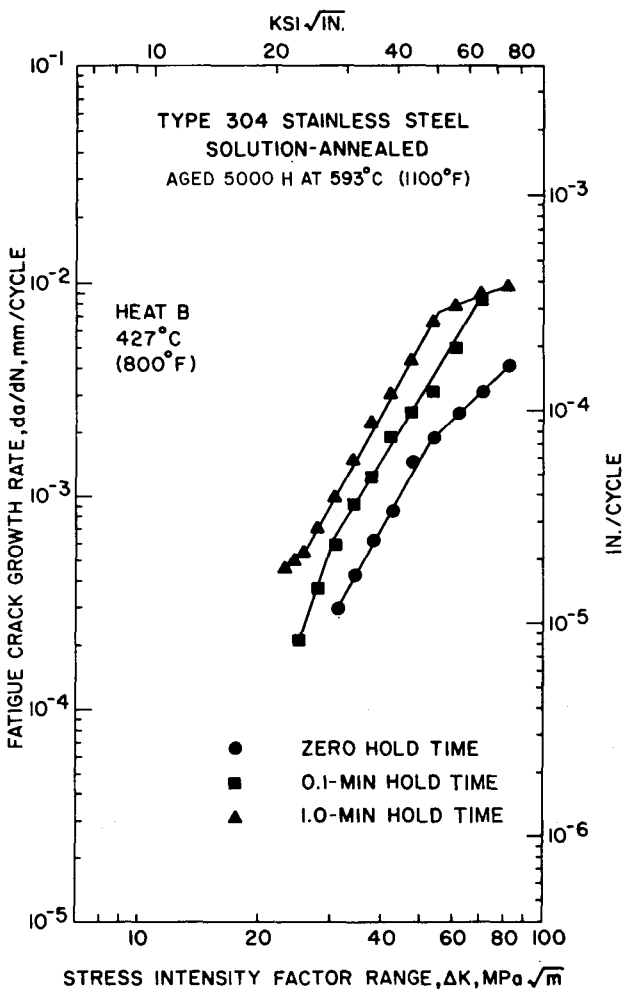

Fig. 7 — Effect of hold time on fatigue crack propagation behavior in air at 427°C for solution-annealed, aged Type 304 stainless steel, Heat B.

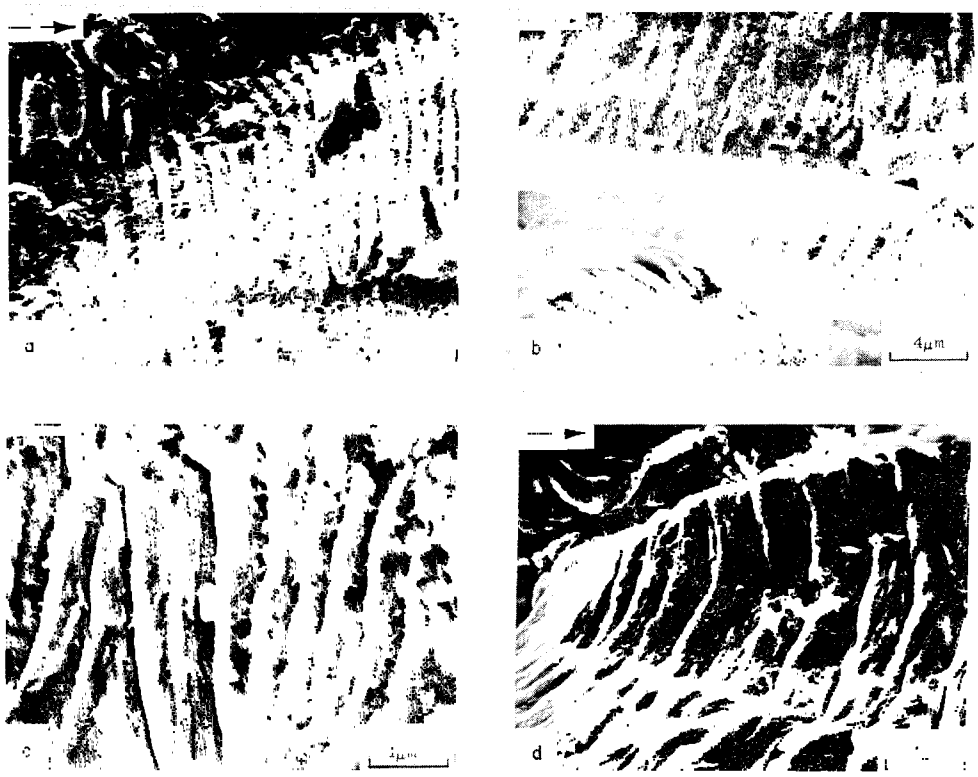

Fig. 8 — Fracture surfaces of a solution-annealed, aged Type 304 stainless steel specimen, Heat B, tested at 427°C without hold time. The SEM micrographs were taken at crack lengths that correspond to the following ΔK values: (a) 22 MPa$\sqrt{m}$ (20 ksi$\sqrt{in.}$), (b) 33 MPa$\sqrt{m}$ (30 ksi$\sqrt{in.}$), (c) 44 MPa$\sqrt{m}$ (40 ksi$\sqrt{in.}$), and (d) 33 MPa$\sqrt{m}$ (30 ksi$\sqrt{in.}$). Arrows show direction of macroscopic crack growth rate. The micrographs show that the specimen failed transgranularly for all values of ΔK.

by fatigue striations whose average spacing increases with ΔK. Rather surprisingly, the specimens with hold times of 0.1 min and 1.0 min exhibited the same basic fractographic features as the specimen with no hold period. The micrographs in Fig. 9 show that the fracture mode for both 0.1- and 1.0-min hold-time tests were transgranular with clear striation markings.

Heat B, Solution-annealed, Aged for 5000 h at 593°C, Tested at 593°C

The macroscopic growth rates of aged, solution-annealed, Heat B material tested at 593°C are shown in Fig. 10. The growth rate for the specimen tested without hold time went from 5×10^{-3} mm/cycle (2×10^{-5} in./cycle) at 22 MPa$\sqrt{m}$ (20 ksi$\sqrt{in.}$) to 1.3×10^{-2} mm/cycle (3×10^{-4} in./cycle) at 77 MPa$\sqrt{m}$ (70 ksi$\sqrt{in.}$). In general, the above growth rate is slightly faster than the growth rate found at 427°C for the same aging treatment (refer to Fig. 5). Imposition of a 0.1-min hold time produced a faster growth rate

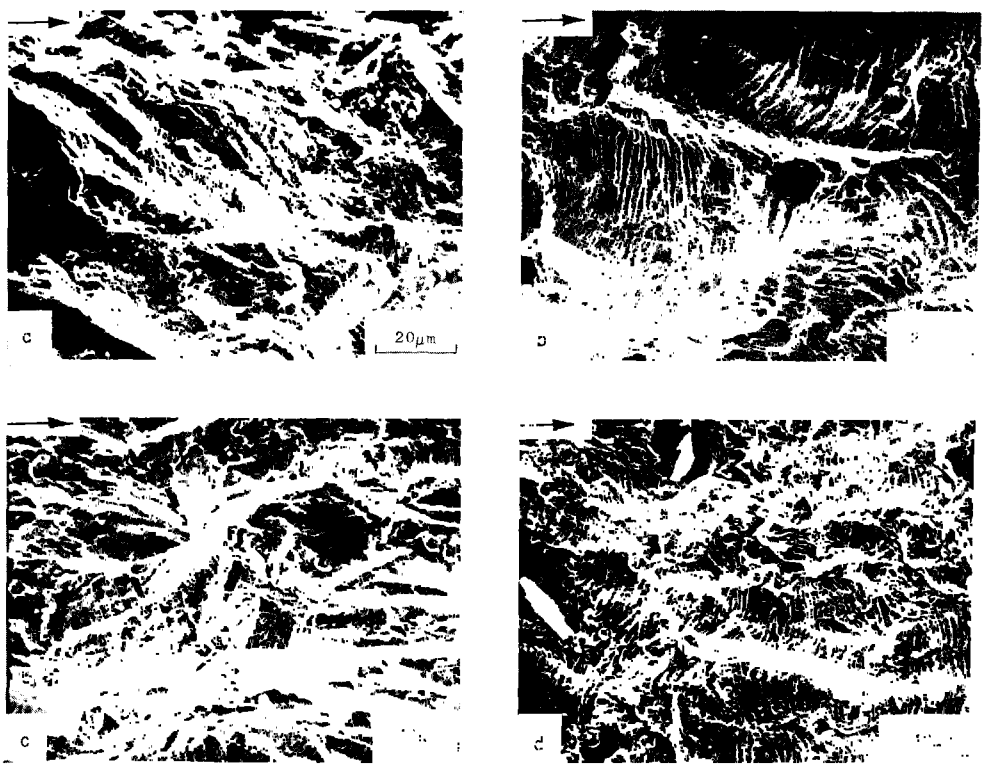

Fig. 9 — Fracture surfaces of solution-annealed and aged Type 304 stainless steel specimens, Heat B, tested at 427°C. Micrographs (a) and (b) refer to the specimen with 0.1-min hold time, while (c) and (d) refer to the specimen with 1-min hold time. The SEM micrographs were taken at crack lengths corresponding to the following ΔK values: (a) 22 MPa$\sqrt{m}$ (20 ksi$\sqrt{in.}$), (b) 33 MPa$\sqrt{m}$ (30 ksi$\sqrt{in.}$), (c) 22 MPa$\sqrt{m}$ (20 ksi$\sqrt{in.}$), and (d) 33 MPa$\sqrt{m}$ (30 ksi$\sqrt{in.}$). Arrows show direction of macroscopic crack propagation. The micrographs show that both specimens fail transgranularly; fatigue striations whose average spacing increases with ΔK are visible in all micrographs.

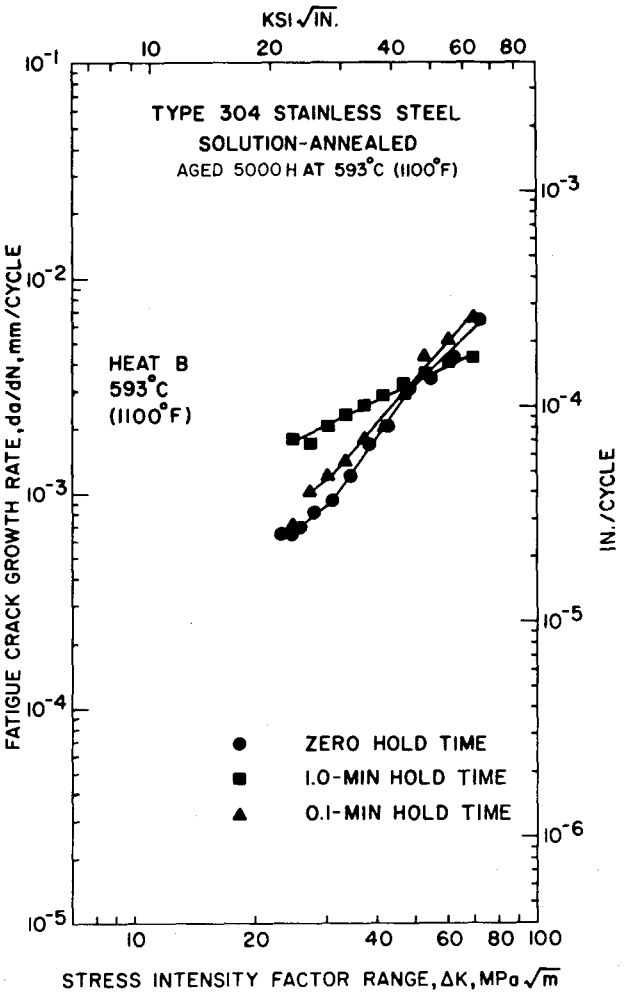

Fig. 10 — The effect of hold time on fatigue propagation rates, da/dN, in air at 593°C for solution-annealed, aged Type 304 stainless steel, Heat B.

in the ΔK region below about 49.5 MPa$\sqrt{m}$ (45 ksi$\sqrt{in.}$) and a slower growth rate above 49.5 MPa$\sqrt{m}$, i.e., a lower slope. Rather surprisingly, the 1.0-min hold-time test had less increase in growth rate at low ΔK than the 0.1-min hold time, and nearly paralleled the zero-hold-time curve above 40 MPa$\sqrt{m}$ (36.4 ksi$\sqrt{in.}$).

Examination of the fracture surfaces of the aged material, Heat B, tested at 593°C shows that the failure mode of the zero hold-time (Fig. 11, a and b) and 0.1-min hold-time (Fig. 11, c and d) specimens was basically transgranular with striation markings observed for all ranges of ΔK. Prominent regions where void coalescence had occurred were present in the 0.1-min hold-time specimens (Fig. 11, d). The specimen with 1-min hold time (Fig. 12) showed patches of intergranular failure in the low-ΔK region (Fig. 12, a and b), but in the higher ΔK region (Fig. 12, c and d) the mode of failure was exclusively transgranular.

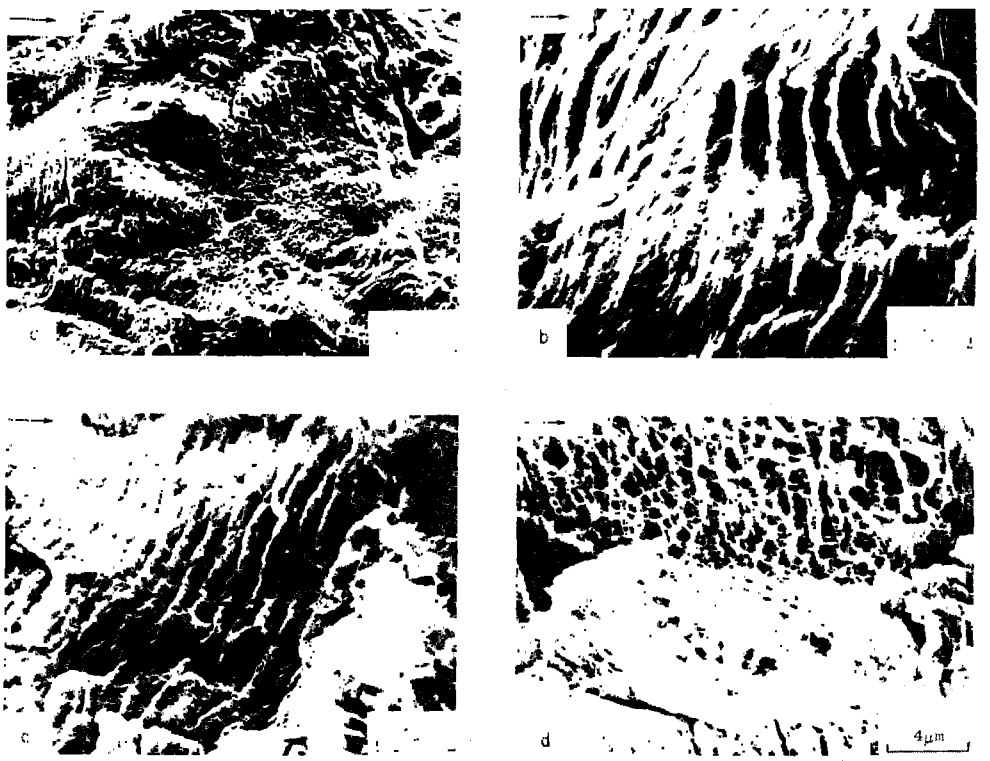

Fig. 11 — Fracture surfaces of solution-annealed, aged Type 304 stainless steel specimens, Heat B, tested at 593°C. Micrographs (a) and (b) of specimen tested with no hold time, (c) and (d) of specimen tested with 0.1-min hold time. The SEM micrographs were taken at crack lengths that correspond to the following values of ΔK: (a) 27.5 MPa$\sqrt{m}$ (25 ksi$\sqrt{in.}$), (b) 44 MPa$\sqrt{m}$ (40 ksi$\sqrt{in.}$), (c) 22 MPa$\sqrt{m}$ (20 ksi$\sqrt{in.}$), and (d) 27.5 MPa$\sqrt{m}$ (25 ksi$\sqrt{in.}$). Arrows show direction of macroscopic crack propagation. The micrographs show that the two specimens fail transgranularly, partially by microvoid coalesence.

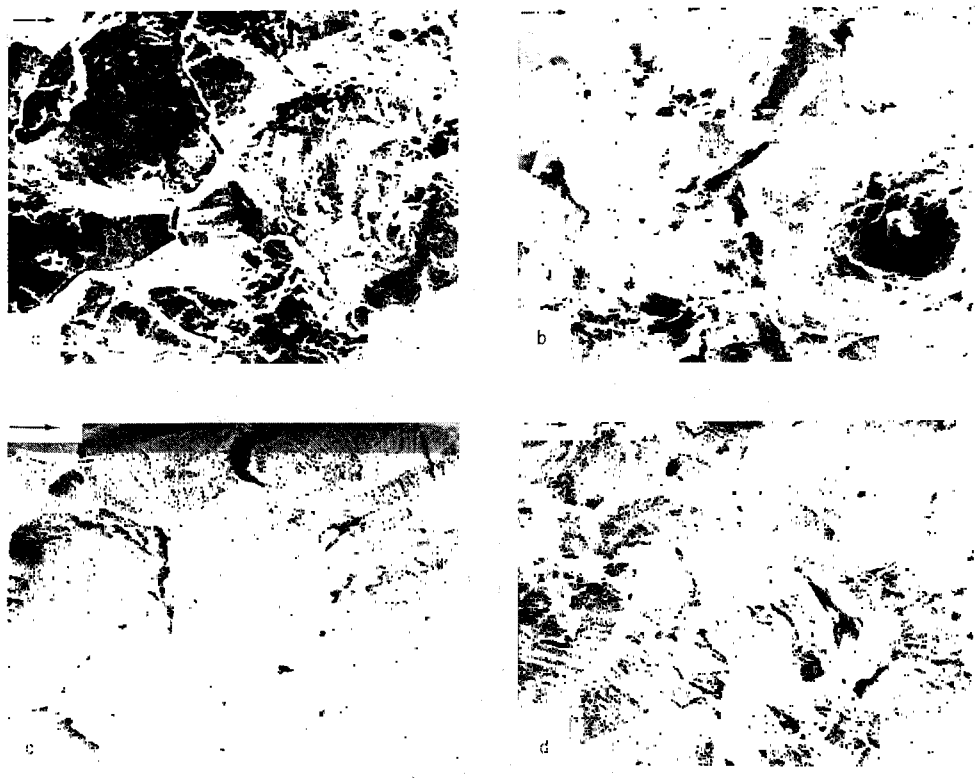

Fig. 12 — Fracture surfaces of a solution-annealed, aged Type 304 stainless steel specimen, Heat B, tested at 593°C with 1-min hold time. The SEM micrographs were taken at crack lengths that correspond to the following ΔK values: (a) 22 MPa$\sqrt{m}$ (20 ksi $\sqrt{in.}$), (b) 27.5 MPa$\sqrt{m}$ (25 ksi$\sqrt{in.}$), (c) 33 MPa$\sqrt{m}$ (30 ksi$\sqrt{in.}$), and (d) 44 MPa $\sqrt{m}$ (40 ksi$\sqrt{in.}$). Arrows show direction of macroscopic crack propagation. The micrographs show that the failure mode was mixed — intergranular and transgranular — in the low-ΔK region and completely transgranular with clear fatigue striations in the high-ΔK region.

Heat A, Solution-annealed, and Solution-annealed and Aged for 5000 h at 593°C, tested at 593°C

Crack growth rate data for SA material from Heat A, tested at 593°C, are shown in Fig. 13. The crack growth rate for the test with no hold time increased from 1×10^{-4} mm/cycle (4×10^{-6} in./cycle) at 14.3 MPa$\sqrt{m}$ (13 ksi$\sqrt{in.}$) to 2.4×10^{-3} mm/cycle (6×10^{-5} in./cycle) at 40 MPa$\sqrt{m}$ (36.4 ksi$\sqrt{in.}$). The crack growth rate is nearly linear over the above range. The introduction of 1-min hold time during the fatigue cycle increased the crack growth rate by about an order of magnitude as compared to the test with no hold time.

Typical SEM micrographs of the SA specimen, Heat A, tested with no hold time, are shown in Fig. 14. As illustrated in the low magnification micrograph taken in the low-ΔK region (Fig. 14, a), the fracture surface showed a mixed mode of failure: transgranular and intergranular. The high magnification micrographs, representative of the

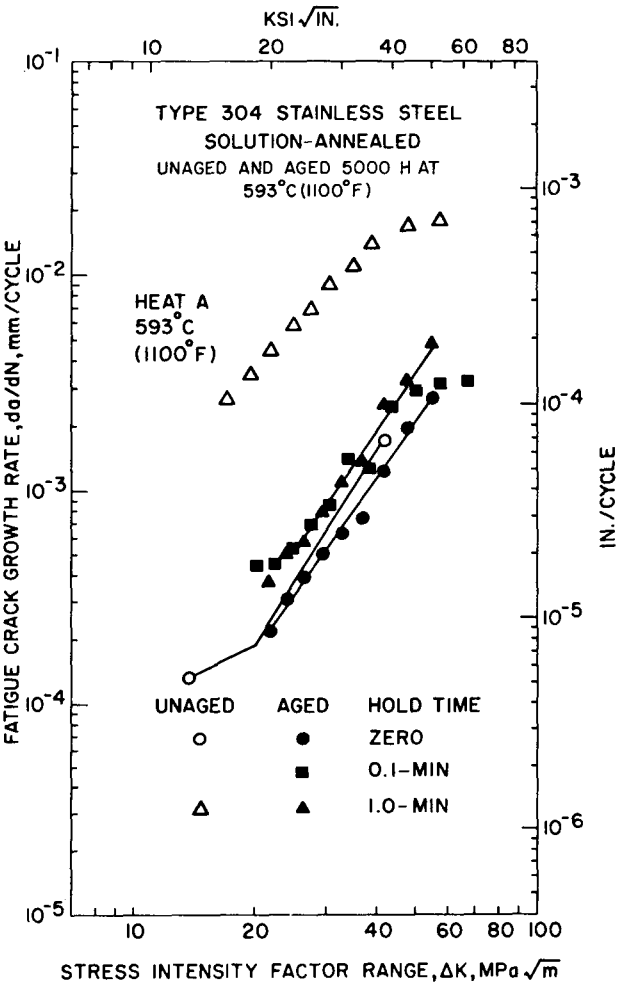

Fig. 13 — Effect of hold time on fatigue propagation rate, da/dN, in air at 593°C for solution-annealed, and solution-annealed and aged, Heat A material.

higher ΔK regime of the test (Fig. 14, b-d) show a transgranular failure mode with fatigue striations. The imposition of a 1-min hold time caused the material to fail by a predominantly intergranular mode for all values of ΔK, as illustrated in Fig. 15. Thus the effect of the hold time is readily apparent in both the increase in growth rate and in the transition to intergranular failure.

The fatigue data for the aged material, Heat A, tested at 593°C are also presented in Fig. 13. The data are linear in the log-log plot and approximately equal to the crack growth rate of the SA specimen of the same heat tested without hold time. Hold times up to 1 min produced a slight increase in the growth rate. Thus, the hold-time effect, clearly present in the fatigue data of the SA material, became negligibly small or was completely absent in the aged material from Heat A.

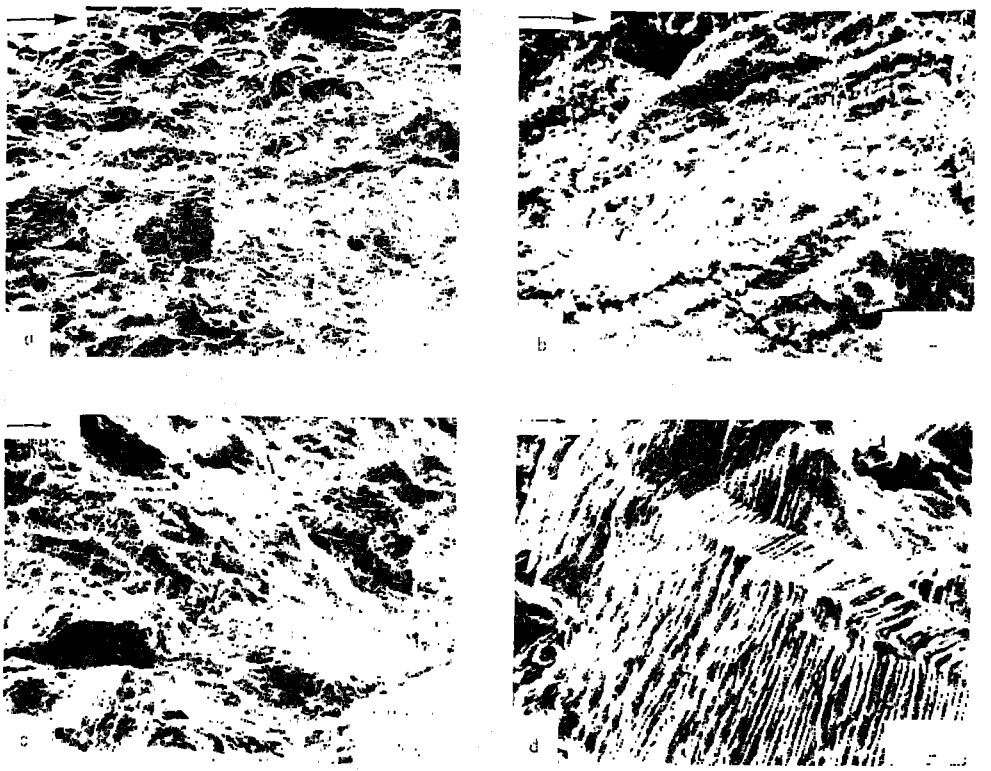

Fig. 14 — Fracture surfaces of a solution-annealed Type 304 stainless steel specimen, Heat A, tested at 593°C without hold time. The SEM micrographs were taken at crack lengths that correspond to the following ΔK values: (a) 22 MPa$\sqrt{m}$ (20 ksi$\sqrt{in.}$), (b) 27.5 MPa$\sqrt{m}$ (25 ksi$\sqrt{in.}$), (c) 33 MPa$\sqrt{m}$ (30 ksi$\sqrt{in.}$), and (d) 44 MPa$\sqrt{m}$ (40 ksi $\sqrt{in.}$). Arrows show direction of macroscopic crack propagation. The mode of fracture is transgranular except for the lowest ΔK region where the fracture mode appears to be mixed — mostly transgranular with intergranular patches.

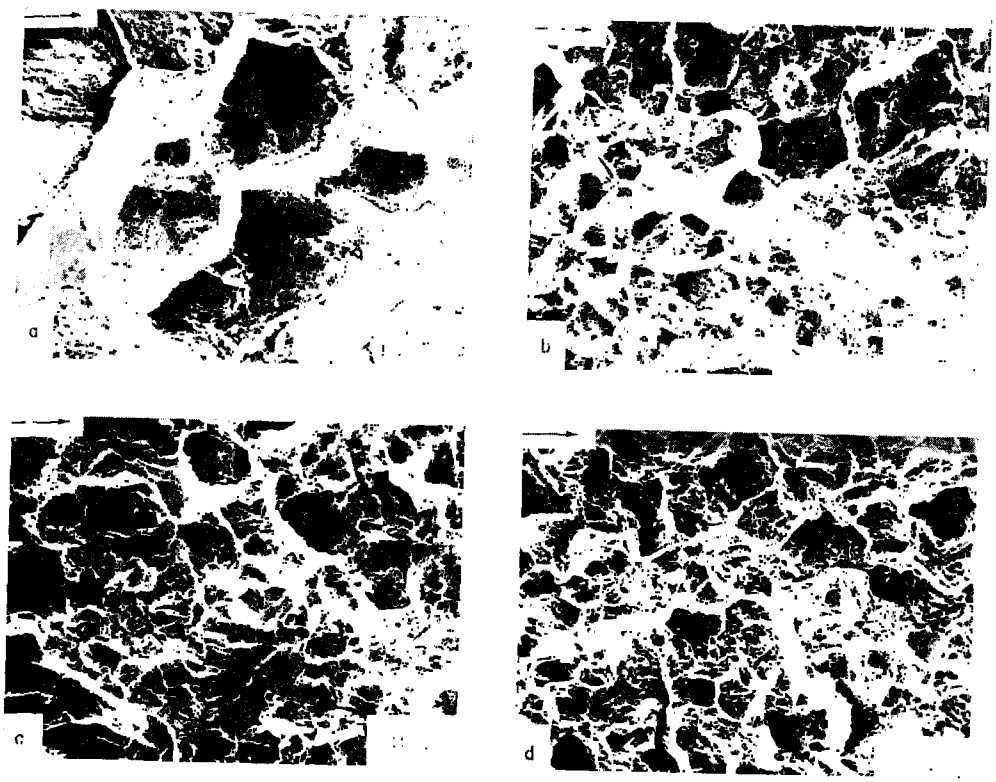

Fig. 15 — Fracture surfaces of a solution-annealed Type 304 stainless steel specimen, Heat A, tested at 593°C with 1-min hold time. The SEM micrographs were taken at crack lengths that correspond to the following ΔK values: (a) 22 MPa$\sqrt{m}$ (20 ksi$\sqrt{in.}$), (b) 27.5 MPa$\sqrt{m}$ (25 ksi$\sqrt{in.}$), (c) 33 MPa$\sqrt{m}$ (30 ksi$\sqrt{in.}$), and (d) 44 MPa$\sqrt{m}$ (40 ksi $\sqrt{in.}$). Arrows show direction of macroscopic crack propagation. As can be seen from the four panels, the specimen failed intergranularly for all values of ΔK.

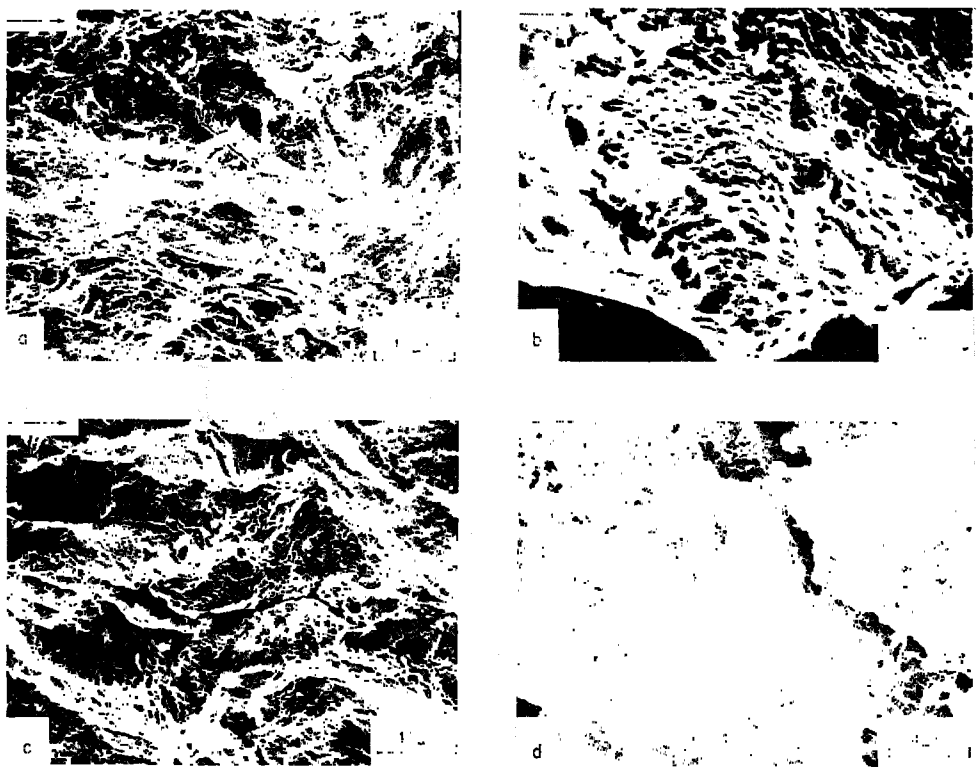

Fig. 16 — Fracture surfaces of a solution-annealed, aged Type 304 stainless steel specimen, Heat A, tested at 593°C without hold time. The SEM micrographs were taken at crack lengths that correspond to the following ΔK values: (a) 22 MPa$\sqrt{m}$ (20 ksi$\sqrt{in.}$), (b) 27.5 MPa$\sqrt{m}$ (25 ksi$\sqrt{in.}$), (c) 33 MPa$\sqrt{m}$ (30 ksi$\sqrt{in.}$), and (d) 44 MPa$\sqrt{m}$ (40 ksi$\sqrt{in.}$). Arrows show direction of macroscopic crack propagation. The specimen failed transgranularly mostly through microvoid coalescence for all values of ΔK.

Typical SEM micrographs of the aged specimen, Heat A, tested at 593°C with no hold time are shown in Fig. 16. The failure mode was transgranular for all values of ΔK. Especially in the higher ΔK region, the fracture surface was characterized by the presence of secondary cracking and shear dimples (Fig. 16, c and d). Imposition of hold times up to 1 min did not appreciably change the microstructure appearance (Fig. 17).

Heat A, 25% Cold-Worked, and 25% Cold-worked and Aged for 5000 h at 593°C, Tested at 593°C

The fatigue data for the 25% cold-worked material, Heat A, tested at 593°C, are shown in Fig. 18. The data are nearly linear in the log-log plot except for a slight change in the slope at 46 MPa$\sqrt{m}$ (41.8 ksi$\sqrt{in.}$). Imposition of a 1-min hold time during the fatigue cycle resulted in an increase in the crack growth rate by approximately 1-2 orders of magnitude compared to the specimen tested without hold time. The above crack growth rate values of the cold-worked specimen tested with 1-min hold time were about one order of magnitude higher than the corresponding values for the crack growth rate of the SA specimen, Heat A, tested at the same temperature, 593°C, with the same hold-time period.

SEM examination of the fracture surface of the cold-worked specimen tested with 1-min hold time shows that the failure mode was largely intergranular, as illustrated in Fig. 19. The grain facets of this specimen were characterized by slip steps that are indicative of the local plastic deformation produced by the cold work. Unfortunately, the 25% cold-worked specimen tested without hold time could not be examined with the SEM because its fracture surface was severely damaged by oxidation.

The fatigue crack propagation data for the 25% cold-worked material aged and tested at 593°C are also shown in Fig. 18. The growth rate for the cold-worked and aged specimen tested with no hold time is slightly higher than the growth rate of the cold-worked material tested at 593°C with no hold time. Impsoition of 0.1- and 1-min hold time in the cold-worked and aged specimens caused an increase in the growth rates over the most of the ΔK range relative to the zero-hold-time test. Changes in the slope occur in all three log da/dN vs log ΔK curves and at different values of ΔK. For comparable values of ΔK, the growth rates of the 25% cold-worked and aged specimens fall between the growth rate of the 25% cold-worked material with 1-min hold time and that of the 25% cold-worked specimen tested without hold time (Fig. 18).

As illustrated by the SEM micrographs in Fig. 20, the fracture surface morphology of the 25% cold-worked and aged specimen tested at 593°C with 0.1-min hold time showed that the mode of failure was partly transgranular and partly intergranular for all values of ΔK. As was the case with the cold-worked specimen, some grain facets were characterized by slip steps running parallel to the macroscopic crack growth direction, thus indicating that a substantial amount of plastic deformation had occurred. An increase in the hold time from 0.1 to 1 min produced no significant change in the fractographic features, as illustrated in Fig. 21. The specimen tested without hold time could not be examined with the SEM because its fracture surface was severely damaged by oxidation, so no comparison with the zero-hold-time specimen was possible.

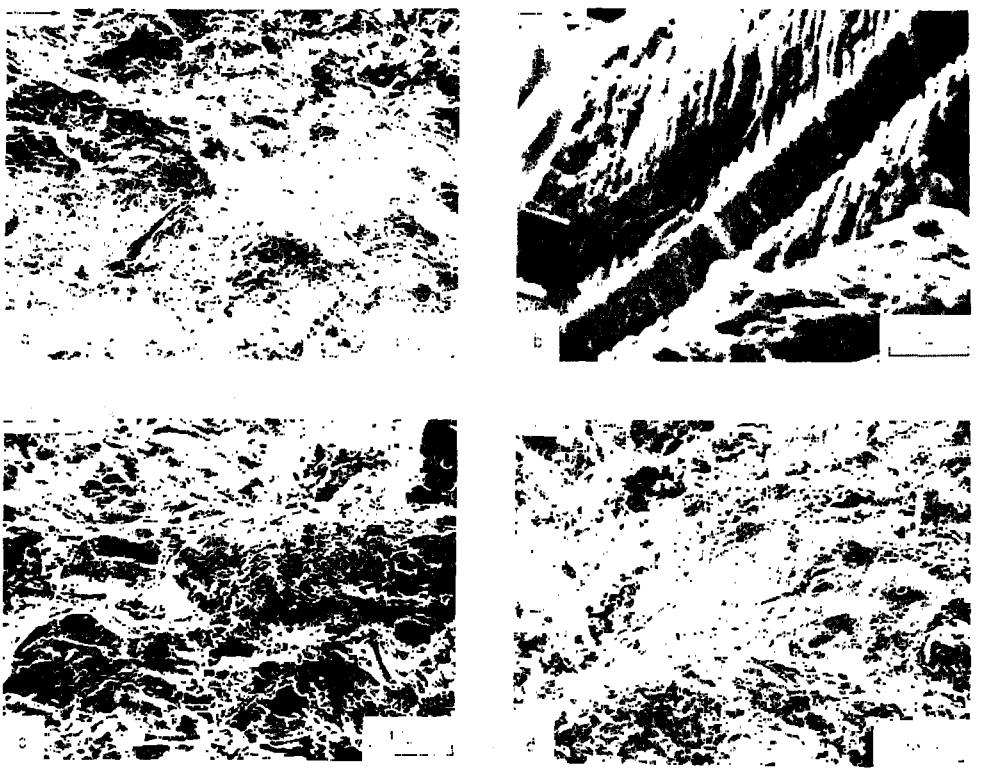

Fig. 17 — Fracture surfaces of solution-annealed, aged Type 304 stainless steel specimens, Heat A, tested at 593°C with 0.1-min ((a) and (b)) and 1.0-min ((c) and (d)) hold times. The SEM micrographs were taken at crack lengths that correspond to the following ΔK values: (a) 22 MPa$\sqrt{m}$ (20 ksi$\sqrt{in.}$) (b) 27.5 MPa$\sqrt{m}$ (25 ksi$\sqrt{in.}$), (c) 22 MPa$\sqrt{m}$ (20 ksi$\sqrt{in.}$), and (d) 27.5 MPa$\sqrt{m}$ (25 ksi$\sqrt{in.}$). Arrows show direction of macroscopic crack propagation. The failure mode was transgranular for both specimens for all values of ΔK. Microvoids can be seen where the oxide layer has been removed, while the topography of fatigue striations is visible where an oxide layer still covers the fracture surface.

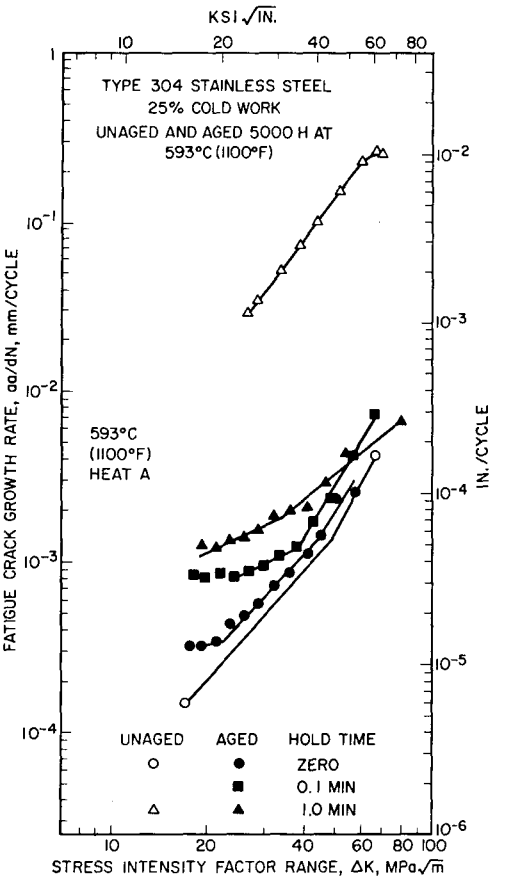

Fig. 18 — Effect of hold time on fatigue propagation rates of solution-annealed Type 304 stainless steel, Heat A, 25% cold-worked, and 25% cold-worked and aged, tested at 593°C.

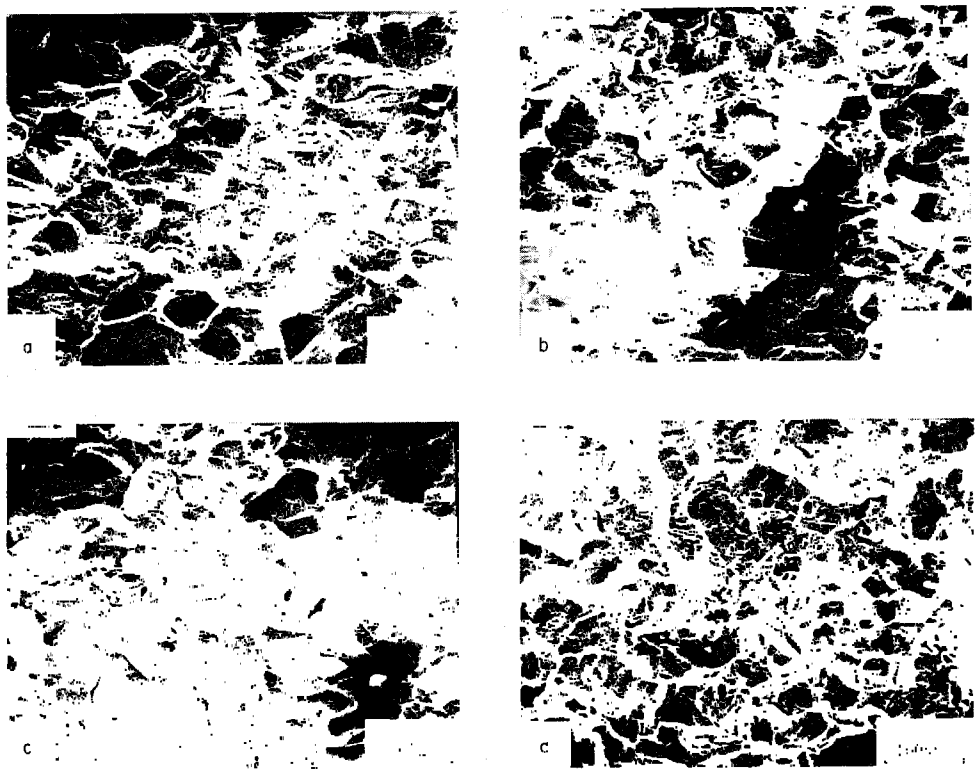

Fig. 19 — Fracture surfaces of a Type 304 stainless steel specimen, Heat A, 25% cold-worked and tested at 593°C with 1.0-min hold time. The SEM micrographs were taken at crack lengths that correspond to the following values of ΔK: (a) 22 MPa$\sqrt{m}$ (20 ksi $\sqrt{in.}$), (b) 27.5 MPa$\sqrt{m}$ (25 ksi$\sqrt{in.}$), (c) 33 MPa$\sqrt{m}$ (30 ksi$\sqrt{in.}$), and (d) 44 MPa$\sqrt{m}$ (40 ksi$\sqrt{in.}$). Arrows show direction of macroscopic crack propagation. The micrographs show that the failure mode is predominantly intergranular for all types of ΔK. The grain facets appear to be elongated and slip steps, indicative of local plastic deformation, are also present.

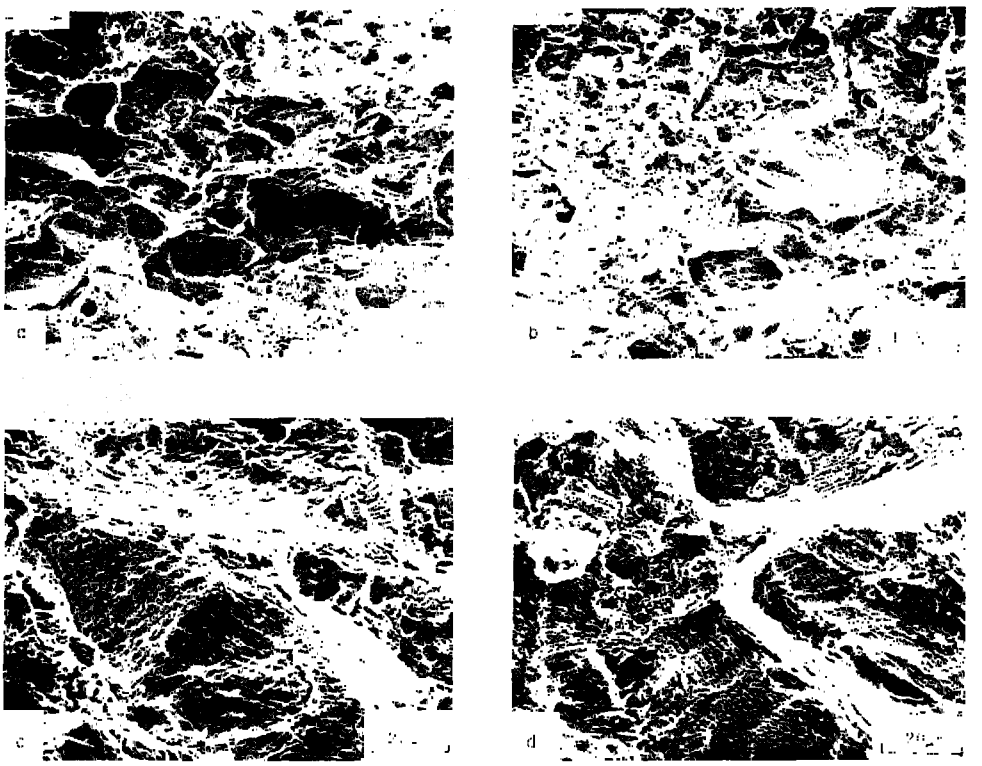

Fig. 20 — Fracture surfaces of a Type 304 stainless steel specimen, Heat A, 25% cold-worked and aged, tested at 593°C with 0.1-min hold time. The SEM micrographs were taken at crack lengths that correspond to the following values of ΔK: (a) 27.5 MPa$\sqrt{m}$ (25 ksi$\sqrt{in.}$), (b) 44 MPa$\sqrt{m}$ (40 ksi$\sqrt{in.}$), (c) 27.5 MPa$\sqrt{m}$ (25.ksi$\sqrt{in.}$), and (d) 44 MPa$\sqrt{m}$ (40 ksi$\sqrt{in.}$). Arrows show direction of macroscopic crack propagation. The failure mode was mixed — transgranular and intergranular — in the entire crack path. Slip steps are also present in most grain facets.

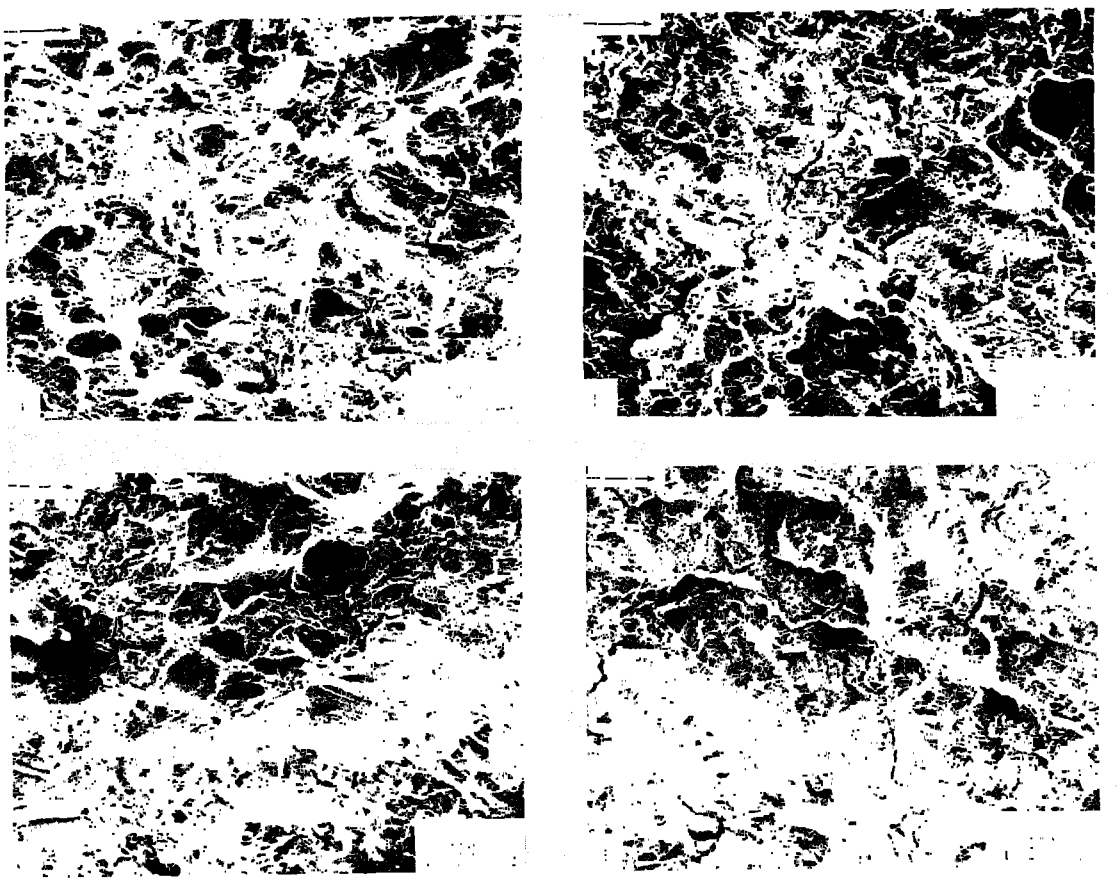

Fig. 21 — Fracture surfaces of a Type 304 stainless steel specimen, Heat A, 25% cold-worked and aged, tested at 593°C with 1.0-min hold time. The SEM micrographs were taken at crack lengths that correspond to the following values of ΔK: (a) 22 MPa$\sqrt{m}$ (20 ksi$\sqrt{in.}$), (b) 27.5 MPa$\sqrt{m}$ (25 ksi$\sqrt{in.}$), (c) 33 MPa$\sqrt{m}$ (30 ksi$\sqrt{in.}$), and (d) 44 MPa$\sqrt{m}$ (40 ksi$\sqrt{in.}$). Arrows show direction of macroscopic crack propagation. The failure mode was mixed — intergranular and transgranular — in the entire crack path.

DISCUSSION

The results of the present study of the fractographic features of Type 304 stainless steel provide additional information for the characterization and interpretation of the high-temperature fatigue behavior of materials. The mechanisms of high-temperature fatigue are not easy to establish because of the difficulty in separating the cyclic components of crack growth rate from time-dependent components and in identifying the contributions of creep and time-dependent environmental attack to the time-dependent growth rate. The latter distinction would be aided by vacuum or inert atmosphere tests of the material, but unfortunately such tests were beyond the scope of the present investigation.

A model was developed to rationalize the crack growth rate data and fractographic evidence in the previous study of Type 316 stainless steel (1). This model was based on a numer of observations reported in the literature and on the 316 observations. The following studies provided relevant observations for the model. Spiedel (8), in an excellent review paper, showed that fatigue tests conducted in air typically reveal an increase in crack growth rate by a factor of 2 or 3 relative to tests conducted in vacuum. At room temperature this increase in growth rate usually did not change the slope of the log da/dN vs log ΔK curves, but simply translated the curves to faster growth rates. At high temperatures, under conditions where oxidation is severe, additional increases in growth rate often occurred, frequently accompanied by the onset of intergranular failure. James (9) showed that for tests conducted in vacuum or in an inert environment, the fatigue crack propagation rate increased only slightly when the test temperature was raised from room temperature to 650°C (1200°F). In contrast to the data in vacuum, data from tests in air showed an increase in the growth rate with increasing temperature. Smith et al. (10) investigated the crack growth rate in Type 316 stainless steel in oxygen environments at 500°C (932°) and at 800°C (1472°F) at pressures ranging from 1.33×10^{-4} Pa to 1.08×10^{5} Pa (10^{-6} torr to 810 torr). They found that crack growth rates were generally 1 to 2 orders of magnitude lower in vacuum than at high oxygen pressure. In summary, these observations showed that testing in air produced an increase in crack growth rate by a factor of 2 to 3 at room temperature, and that growth rate was only slightly temperature-dependent in vacuum or inert evniornment tests, but more strongly temperature-dependent in air.

The previous work on Type 316 stainless steel (1) showed that an increase in test temperature from 427° to 593°C in the air environment caused a change in fracture mode in the low-ΔK (slow growth rate) portion of the test from transgranular with striation markings to intergranular. This change also increased the crack growth rate. Imposition of a hold time extended the range of ΔK over which intergranular fracture was observed and further increased the crack growth rate. Material aged 5000 h at 593°C and tested at 593°C did not show intergranular failure and had the same crack growth rate as the SA specimens tested at 427°C.

The model proposed to explain these observations is that the adsorption of oxygen on the crack surface causes the increase in crack growth rate seen in comparing vacuum or inert atmosphere results to those in air. This initial increase in rate is only slightly temperature-dependent up to at least 427°C and is possibly due to a change in bond energy at the crack tip, which reduces the energy to produce new surface area. At some

temperature between 427° and 593°C, oxygen diffusion along the grain boundaries is rapid enough to exceed the crack growth rate, and another increment in crack growth rate and a change in fracture mode to intergranular failure takes place. Imposition of a hold time increases the time between cycles and hence the diffusion distance of the oxygen between cycles. A corresponding increase in crack growth rate and the range of growth rates over which intergranular failure can occur correlates well with the kinetics of intergranular diffusion. Aging the material has the effect of strengthening the grain boundaries relative to the matrix so that they are no longer the point of failure even though oxygen presumably is diffusing along the interface.

The results of the present study of Type 304 stainless steel closely paralleled those of the previous study on Type 316 stainless steel. Solution-annealed material tested at 427°C showed a transgranular fracture mode with striation markings. Hold times up to 1.0 min had no effect on the crack growth rate or the appearance of the fracture surface at 427°C. Increasing the testing temperature from 427° to 593°C increased the crack growth rate by an order of magnitude at comparable values of ΔK and led to a mixed-mode fracture at low ΔK with a transition to completely transgranular above the ΔK level of 33 MPa$\sqrt{m}$ (30 ksi$\sqrt{in.}$). Imposition of 0.1- and 1.0-min hold times increased the proportion of the fracture surface characterized by intergranular failure. These observations on the SA heat B material are consistent with the model of grain boundary embrittlement by oxygen previously set forth.

Results for the aged specimen of Type 304 tested at 427°C showed a crack growth rate approximately the same as for the SA material. Imposition of hold times up to 1 min progressively increased the growth rates to levels that are on the average a factor of 3 higher than the growth rate of the zero-hold-time test (Fig. 7). This result differs from the behavior of Type 316 stainless steel (1), where no hold-time effect was observed in the aged material tested either at 427°C or at 593°C for hold times up to 1 min. Tests on Type 304 aged material at 593°C also showed an increase in crack growth over the tests at 427°C. The data for 0.1-min hold time at 593°C were unusual in showing a lower slope than either the zero or 1-min hold-time data. In fact, the 0.1-min hold-time curve had a higher rate (by a factor of about 2-3) at lower ΔK, and a lower rate than the other two tests in the high-ΔK region. These results differ from those on aged Type 316 stainless steel in that an increase in crack growth rate over that for the 427°C SA crack growth rates was observed in aged material.

SEM examination of the fracture surfaces of the aged specimens tested at 427°C showed a transgranular fracture path for all values of ΔK (Figs. 8 and 9). Transgranular failure was also observed in the fracture surfaces of the two aged specimens tested at 593°C (Fig. 11), with the exception of the 1-min hold-time test where the failure mode was mixed — transgranular and intergranular — in the low-ΔK region (Fig. 12, a and b). Regions where failure had occurred by microvoid coalescences were observed on the fracture surfaces of all aged specimens tested at 593°C. The voids appeared to have formed at precipitate particles believed to be carbides (Fig. 11, a and d). The fractographic evidence supported the model for increased crack growth rate due to grain boundary embrittlement and intergranular failure in some of these cases but not in others. The observations for the tests at 427°C, zero hold-time (transgranular) and at 593°C, 1-min hold-time (intergranular) were consistent with the model, while the 427°C,

0.1- and 1-min hold-time (faster growth rate, but transgranular) and 593°C, zero hold-time (faster growth rate, but transgranular) observations did not support the model. The 593°C, 0.1-min hold-time test was unusual, and should be repeated before attributing any significance to the observed behavior.

The behavior of the aged Type 304 stainless steel showed the reduced tendency for carbide formation in this material compared to Type 316 stainless steel (0.048 vs 0.060 weight percent carbon), and was indicative of a borderline behavior where the grain boundary strengthening sometimes prevents intergranular crack propagation and sometimes does not. Grain boundary orientation relative to the advancing crack front may also have influenced the occurrence of grain boundary failure.

The fatigue behavior of the SA material from Heat A tested at 593°C was entirely consistent with the observations on Heat B under the same conditions and with the model The behavior of the aged material was surprising, however, in that it resembled the Type 316 stainless steel and did not exhibit the "borderline behavior" just discussed for Heat B. There were no obvious differences in composition or heat treatment that would explain the contrary behavior of Heats A and B. More extensive testing with careful control of the heat treatment and a reanalysis of the compositions would be necessary to determine the factors involved.

The fatigue crack growth rate of 25% cold-worked Type 304 steel, Heat A, tested at 593°C without hold time was comparable to the crack growth rate of SA Type 304 steel without hold time (Figs. 13 and 18). The introduction of a 1-min hold time resulted in an acceleration of the crack growth rate by about two orders of magnitude. The fatigue crack growth behavior of the cold-worked and aged material, also summarized in Fig. 18, showed that the growth rate was slightly higher than the growth rate of the corresponding cold-worked specimen. Imposition of hold times up to 1 min progressively increased the crack growth rate, but not as much as in the cold-worked specimen. The failure mode for the cold-worked specimen tested with 1-min hold time was largely intergranular for the entire crack path (Fig. 19). Slip steps, indicative of local plastic deformation, were present on most grain facets (Fig. 19). The failure mode was mixed for the cold-worked and aged specimens tested at 593°C with 0.1- and 1-min hold times. Slip steps were also present on the fracture surfaces of the aged specimens.

The largely intergranular failure mode and the accelerated crack growth rate observed in the cold-worked specimen tested at 593°C with 1-min hold time can be rationalized with the model by attributing the major effect of cold work to strengthening the matrix material relative to the grain boundaries. The aging treatment produces some strengthening of the grain boundaries, but less grain boundary precipitation occurs because the cold work provides more nucleation sites for precipitates in the matrix. In addition, partial recovery of the cold work during the aging treatment may also reduce the strength of the matrix relative to the grain boundaries.

The present results on Type 304 stainless steel have been shown to be consistent with the previous patterns observed in Type 316 stainless steel, with the possible exception of the Heat B material; in the aged condition, Heat B material sometimes showed sufficient grain boundary strenthening to prevent intergranular failure and sometimes did

not. The behavior of Heat B differed from that of a companion Heat A, but the origins of the difference were not apparent in either the composition or the heat treatments given the two materials. An additional variable in the form of cold work was investigated in the Type 304 material, and the principal effect was found to be a strengthening of the matrix relative to the grain boundaries, which accelerated the crack growth rate and increased the extent of intergranular failure.

SUMMARY AND CONCLUSIONS

SEM examination of fracture surfaces of fatigue specimens of Type 304 stainless steel previously tested at elevated temperatures (2-4) has provided some useful insight into the crack propagation behavior of this material. The specimens examined were of two different heats (Heat A and Heat B) with slightly different alloy composition. Tests were performed on the following combinations of test conditions and material history: (a) Heat B, solution-annealed, tested at 427°C, (b) Heat A and Heat B solution-annealed, tested at 593°C, (c) Heat B, aged for 5000 h at 593°C, tested at 427°C, (d) Heat A and Heat B, aged for 5000 h at 593°C, tested at 593°C, (e) Heat A, 25% cold-worked tested at 593°C, and (f) Heat A, 25% cold-worked, aged for 5000 h at 593°C, tested at 593°C. Hold-time tests of 0.1 and 1 min were also conducted for each combination. The results of the present study can be summarized as follows:

- Heat B, SA material, tested at 427°C, exhibited a transgranular failure mode with fatigue striations indicative of a ductile failure process.

- Solution-annealed material of both Heat A and Heat B, tested at 593°C, showed patches of intergranular failure in the low-ΔK range of the test. For the Heat B material for which a direct comparison was possible (SA material, Heat A, was not tested at 427°C), the crack growth rate at 593°C was higher than the rates at 427°C. In both materials, imposition of hold times up to 1 min further increased the crack growth rate and the proportion of the fracture surface characterized by intergranular failure.

- Heat B in the material aged condition, tested at 427°C, exhibited a transgranular failure with fatigue striations, but the mechanical data showed an increase in the growth rate with hold time. No obvious fractographic features were observed that would account for the increased crack growth rate. This behavior is not consistent with the pattern observed for other test conditions in either Type 304 or Type 316 stainless steel and should be reexamined before drawing final conclusions.

- Heat A in the aged condition, tested at 593°C, exhibited a transgranular failure mode. It is concluded that aging strengthened the grain boundaries, preventing intergranular failure and reducing the crack growth rate relative to the growth rate of SA material.

- Heat A material in the 25% cold-worked condition, tested at 593°C with 1-min hold time, exhibited an intergranular failure mode. The fatigue data showed a higher growth rate than that of the SA material, and the presence of a large hold-time effect. The cold work appeared to increase the crack growth rate and the proportion of the area characterized by intergranular fracture by strengthening the matrix relative to the grain boundaries.

• Cold-worked and aged specimens of Heat A, tested at 593°C showed transgranular mode failure over the entire crack path. The growth rate of the zero-hold-time test was slightly higher than the growth rate of the cold-worked specimen which had not been aged. Hold-time tests on the cold-worked and aged material progressively increased the crack growth rates by a factor of 3 in the low-ΔK region. These crack growth rates, however, were about an order of magnitude lower than that of the cold-worked specimen tested with 1-min hold time. These observations are believed to be the outcome of competing mechanisms involving grain boundary strengthening by precipitation, and a lower strength matrix due to partial recovery of the cold work.

• These observations on Type 304 stainless steel support the model previously developed to explain the elevated temperature fatigue behavior of Type 316 stainless steel (1). According to this model, the basic fatigue behavior for austenitic stainless steels is observed in vacuum or inert atmosphere tests and consists of transgranular failure by the propagation of fatigue cracks under alternating shear and compression at the crack tip. The presence of oxygen causes an immediate increase in crack growth by factors of 2 to 3, but no change in the failure mode. This appears to be the result of some modification of the bond energy at the crack tip so that the energy to create new surface is lowered. Between 427° and 593°C, diffusion of oxygen along grain boundaries exceeds the rate of crack growth, and the embrittled boundaries lead to intergranular failure. Hold-time tests increase the range of ΔK over which intergranular failure occurs. Strengthening the grain boundaries by aging the material reduces the tendency to intergranular failure, while strengthening the matrix by cold work increases the tendency to intergranular failure.

ACKNOWLEDGMENTS

This work was supported by the U.S. Department of Energy, Division of Reactor Research and Technology. The authors wish to express their appreciation to Dr. J. A. Sprague for helpful discussions on the manuscript and to Dr. D. J. Michel, Dr. P. Shahinian and H. H. Smith for providing the samples from their tests.

REFERENCES

1. F.A. Smidt, Jr. and V. Provenzano, "SEM Observations on Fracture Surfaces of Fatigue Specimens of Annealed Type 316 Stainless Steel," NRL Report 8133, August 10, 1977.

2. P. Shahinian, "Creep-Fatigue Crack Propagation in Austenitic Stainless Steel," Trans. ASME, Vol. J93, pp. 166-172, 1976.

3. D. J. Michel, H. H. Smith, and H. E. Watson, "Effect of Hold-time on Elevated Temperature Fatigue Crack Propagation in Fast Neutron Irradiated and Unirradiated Type 316 Stainless Steel," in *Structural Materials for Service at Elevated Temperature in Nuclear Power Generation*, A.O. Schaefer, ed., MPC-1, ASME, pp. 167-190, 1975.

4. D. J. Michel and H. H. Smith, "Effect of Hold Time on Elevated Temperature Fatigue Crack Propagation in Types 304 and 316 Stainless Steel," in *Symposium on Creep-Fatigue Interactions*, R. M. Curran, Ed. MCP-3, ASME, 1976, pp. 391-415.

5. *SEM/TEM Fractography Handbook*, Battelle Columbus Laboratories, Metals and Ceramics Information Center, MCIC-HB-06, December 1975.

6. B. Gross and J. E. Srawley, "Stress-Intensity Factors for Single Edge-Notch Specimens in Bending or Combined Bending and Tension by Boundary Collocation Function," NASA-TN-D2603, National Aeronautics and Space Administration, Washington, DC, January 1975.

7. C. Laird, ASTM Conf. on Fatigue Crack Propagation, Atlantic City pp. 131-168, 1966.

8. M. O. Speidel, "Fatigue Crack Growth at High Temperature," *High Temperature Materials in Gas Turbines*, Amsterdam, pp. 207-251, 1974.

9. L. A. James, "Fatigue-Crack Propagation in Austenitic Stainless Steels," Atomic Energy Review 14, 37-86, 1976, published by IAEA, Vienna, Austria.

10. H. H. Smith, P. Shahinian, and M. R. Achter, "Fatigue Crack Growth Rates in Types 316 Stainless Steel at Elevated Temperatures as a Function of Oxygen Pressure," Trans. Metall. Soc. AIME, 245, 947-953, 1969.